Flux jumps in high-J_c MgB$_2$ bulks during pulsed field magnetization

H. Fujishiro[1], H. Mochizuki[1], T. Naito[1], M.D. Ainslie[2] and G. Giunchi[3]

[1] Department of Materials Science and Engineering, Faculty of Engineering, Iwate University, 4-3-5 Ueda, Morioka 020-8551, Japan

[2] Bulk Superconductivity Group, Department of Engineering, University of Cambridge, Trumpington Street, Cambridge CB2 1PZ, UK

[3] Materials Science Consultant, via Teodosio 8, 20131 Milano, Italy

Abstract

Pulsed field magnetization (PFM) of a high-J_c MgB$_2$ bulk disk has been investigated at 20 K, in which flux jumps frequently occur for high pulsed fields. Using a numerical simulation of the PFM procedure, we estimated the time dependence of the local magnetic field and temperature during PFM. We analyzed the electromagnetic and thermal instability of the high-J_c MgB$_2$ bulk to avoid flux jumps using the time dependence of the critical thickness, $d_c(t)$, which shows the upper safety thickness to stabilize the superconductor magnetically, and the minimum propagation zone (MPZ) length, $l_m(t)$, to obtain dynamical stability. The values of $d_c(t)$ and $l_m(t)$ change along the thermally-stabilized direction with increasing temperature below the critical temperature, T_c. However, the flux jump can be qualitatively understood by the local temperature, $T(t)$, which exceeds T_c in the bulk. Finally, possible solutions to avoid flux jumps in high-J_c MgB$_2$ bulks are discussed.

1. Introduction

Bulk MgB$_2$ superconductors have a promising potential as quasi-permanent magnets, and have a number of attractive properties, such as being rare-earth-free, light-weight and presenting a homogeneous trapped field distribution, which are in clear contrast with REBaCuO bulk magnets. The problem of weak-links at grain boundaries can be ignored in MgB$_2$ polycrystalline bulks due to their long coherence length, ξ [1]. These characteristics enable us to realize better and larger polycrystalline MgB$_2$ bulk magnets below the transition temperature $T_c = 39$ K, which are expected to be applicable in magnetically levitated trains (MAGLEVs) and wind power generators using liquid H$_2$ or cryocooler systems. Several groups have already reported the trapped field B_z for MgB$_2$ bulks activated by field-cooled magnetization (FCM) [2, 3]. We have attained $B_z = 3.6$ T and 4.6 T at 14 K on a single bulk and in a bulk pair, respectively, for a Ti-doped MgB$_2$ bulk 35 mm in diameter fabricated by a hot isostatic pressing (HIP) method [4]. A record-high trapped field of $B_z = 5.4$ T has been attained at 12 K on a single MgB$_2$ bulk 20 mm in diameter, which was fabricated by hot-pressing of ball-milled Mg and B powders using fine-grained boron powders [5].

Pulsed-field magnetization (PFM) has also been investigated to magnetize such bulk superconductors. However, the trapped field B_z by PFM is generally lower than that by FCM because of a large temperature rise caused by the dynamic motion of the magnetic flux. It is well known that multi-pulse techniques are extremely effective in enhancing B_z for REBaCuO bulks due to the reduction of this temperature rise [6, 7]. We have achieved the highest trapped field of B_z = 5.20 T with a GdBaCuO bulk 45 mm in diameter at 30 K using a modified multi-pulse technique with stepwise cooling (MMPSC) [8], which is a record-high value for a REBaCuO bulk magnetized by PFM to date. The PFM technique has also been performed to MgB$_2$ bulks fabricated by various methods [9, 10]. However, B_z(PFM) = 0.80 T at 14 K is the highest value for an MgB$_2$ bulk fabricated by the HIP method, for which B_z(FCM) = 2.23 T was trapped at 16 K by FCM [11]. The numerical simulation is a valuable technique to understand the mechanism of the flux intrusion and the flux trapping during PFM for REBaCuO and MgB$_2$ bulks [12, 13, 14]. Considering the experimental results and the numerical simulation for the REBaCuO system, the B_z(PFM) value for the MgB$_2$ bulk is expected to be enhanced by using a bulk with a higher B_z(FCM) and/or a higher critical current density, J_c. However, flux jumps took place frequently during PFM in the MgB$_2$ bulk and consequently the B_z(PFM) value decreased for higher applied magnetic fields, which has been scarcely observed for REBaCuO bulks at around 40 K during PFM. Flux jumps are scarcely observed in low-J_c MgB$_2$ bulks and even in high-J_c MgB$_2$ bulks for lower applied fields, B_{ex}. The flux dynamics and heat generation in the MgB$_2$ bulk at around 20 K are in clear contrast with those in the REBaCuO bulk at around 40 K because of the small specific heat, large thermal conductivity, and a narrow temperature margin against T_c for the MgB$_2$ bulk. A concentric-circled MgB$_2$ bulk composite disk is one of the possible solutions to avoid flux jumps by PFM, because many MgB$_2$ thin rings are filled in both surfaces of highly thermal conductive metal disk, and the generated heat is removed quickly [15].

In this study, we analyze and discuss the electromagnetic and thermal instability during PFM of a high-J_c MgB$_2$ bulk fabricated by the HIP method to avoid flux jumps using conventional relations, such as the critical thickness, d_c, and the minimum propagation zone (MPZ) length, l_m.

2. Experimental procedure

A bulk MgB$_2$ superconducting disk was fabricated by a HIP method. The diameter and thickness is 38 mm and 7 mm, respectively, and the relative mass density was as high as 93% of the ideal mass density. The detailed fabrication process is described elsewhere [4]. The bulk MgB$_2$ disk was mounted in a stainless steel ring (38.1 mm I.D., and 56.0 mm O.D.) using epoxy resin (Stycast 2850^{TM}) and was tightly anchored onto the cold stage of a Gifford–McMahon (GM) cycle helium refrigerator. The details of the PFM procedure and experimental setup are described elsewhere [9, 11]. The initial temperature, T_s, of the bulk

was set to 20 K. The solenoid copper magnetizing coil (99 mm I.D., 121 mm O.D., and 50 mm height), which was submerged in liquid nitrogen, was placed outside the vacuum chamber. Magnetic pulses, B_{ex}, up to 2.2 T, with a rise time of 0.013 s and duration of 0.15 s were applied via a pulse current in the coil. The time evolution of the local field, $B_z(t)$, and the subsequent trapped field, B_z, at the center of the bulk surface, which was defined as the final value of $B_z(t)$, were monitored by a Hall sensor (BHA 921; F W Bell). Two-dimensional trapped field profiles of B_z were mapped stepwise with a pitch of 1 mm by scanning the same Hall sensor using an x–y stage controller. During PFM, the time evolution of the temperature, $T(t)$, was measured at the center of the bulk surface using a thermometer (Cernox[TM]; Lakeshore), which was adhered by GE7031[TM] varnish.

After the PFM experiments, the bulk was cut and small pieces about 1 x 1 x 2 mm^3 in size were prepared for magnetization curve $M(H)$ measurements at 10, 20 and 30 K under a magnetic field up to $\mu_0 H = 5$ T using a commercial SQUID magnetometer (MPMS-5 T; Quantum Design). The J_c-B relationship was estimated from the $M(H)$ hysteresis loop using an extended Bean model, $J_c = 20 \Delta M / a(1-a/3b)$, where a and b are the dimensions of the plane of the sample perpendicular to the applied field and ΔM is the width of the $M(H)$ loop. The temperature dependence of the thermal conductivity, $\kappa(T)$, was measured by a steady-state heat flow method.

3. Numerical analysis

Based on the experimental setup, a model for the numerical simulation of PFM was constructed as shown in Fig. 1, in which the physical phenomena occurring during the magnetization process are described using the fundamental electromagnetic and thermal equations in axisymmetric coordinates. The details of the numerical simulation have been described elsewhere [16, 17]. We set a spacing plate 2 mm in thickness with a thermal conductivity of $\kappa_{cont} = 0.5$ Wm^{-1}K^{-1} between the bulk and the cold stage of the refrigerator, which imaginarily represents both the cooling power of the refrigerator and the thermal contact. The power-n model ($n = 100$) was used to describe the nonlinear E-J characteristic of the MgB$_2$ bulk. The measured $J_c(B)$ of the MgB$_2$ bulk at 20 K was fitted using the following equation,

$$J_c(B, T) = \alpha \left\{ 1 - \left(\frac{T}{T_c} \right)^2 \right\}^{\frac{3}{2}} \exp \left[- \left(\frac{B}{B_0} \right)^{\beta} \right], \qquad (1)$$

where $T_c = 39$ K, and $\alpha = 4.5 \times 10^9$ A/m^2, $B_0 = 1.3$ T and $\beta = 1.7$ are the fitted parameters at 20 K. The magnetic field and temperature dependence of the critical current density $J_c(B, T)$ was estimated according to Eq. (1). Iterative calculations were performed for analyzing the combined problem of electromagnetic fields and heat diffusion by the finite element method

(FEM) using commercial software, Photo-Eddy, combined with Photo-Thermo (Photon Ltd., Japan). In the analysis of thermal conduction, the temperature dependence of the thermal conductivity, $\kappa(T)$, and the specific heat, $C(T)$, of the MgB$_2$ and the stainless steel [18] were introduced.
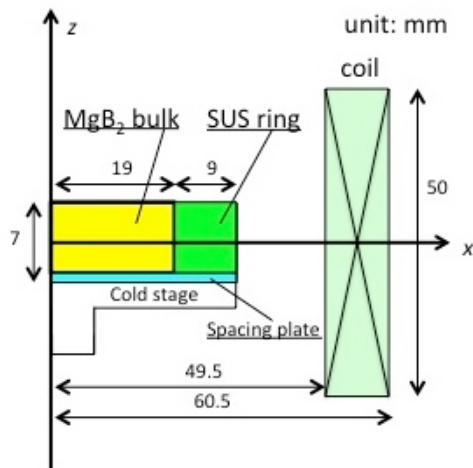

Figure 1. Schematic view of the experimental setup for PFM.

3. Experimental results

Figure 2(a) shows the relationship between the trapped field, B_z, by PFM and the applied pulsed field, B_{ex}, for the MgB$_2$ bulk at $T_s = 20$ K. Similar to the previous experimental results for REBaCuO and MgB$_2$ bulks magnetized by PFM [6, 9], the B_z value increases, attains a maximum value, and then decreases with further increasing B_{ex}. However, for the bulk with a higher J_c, flux jumps took place frequently for higher applied fields.
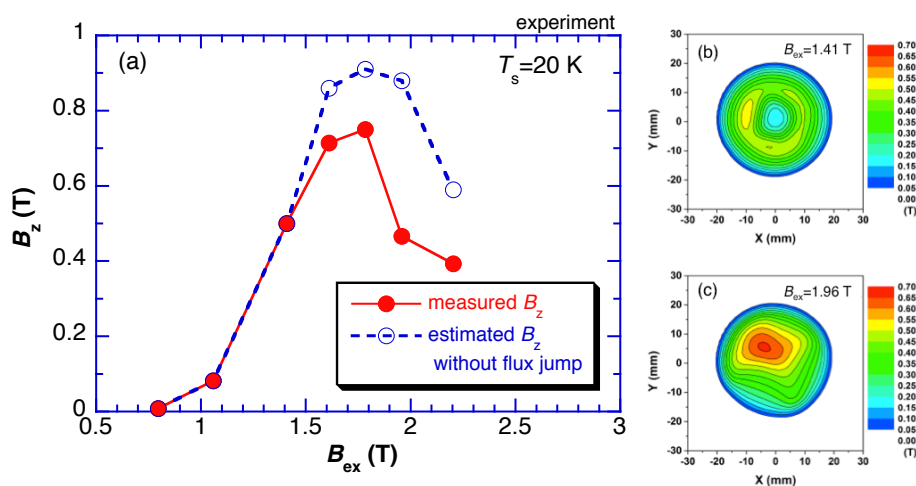

Figure 2. (a) Applied pulsed-field dependence of trapped field, B_z, for the MgB$_2$ bulk at $T_s = 20$ K at the center of the bulk surface. The dashed line shows the estimated B_z value, in the case that no flux jump took place during PFM (see Fig. 3(b)). The trapped field profiles for (b) $B_{ex}=1.41$ T and (c) $B_{ex}=1.96$ T, mapped on the bulk at 1 mm above the bulk surface, are shown.

Figures 3(a) and 3(b) depict the time evolution of the local field, $B_z(t)$, at the center of the bulk surface and the applied pulsed field, $B_{ex}(t)$, for B_{ex} = 1.41 T and B_{ex} = 1.96 T, respectively. For B_{ex} = 1.41 T, $B_z(t)$ started to increase with a slight time delay, took a maximum at 0.016 s, and then decreased smoothly with increasing time. However, for B_{ex} = 1.96 T, $B_z(t)$ saw a slight drop at t = 0.05 s and a larger drop of about 40% at t = 0.07 s due to flux jumps. Then, $B_z(t)$ approaches to the final trapped field, B_z, due to flux creep. The estimated $B_z(t)$ curve is also shown in the figure, which was fitted before the flux jumps using an exponential curve. The estimated $B_z(t)$ introduces the final trapped field, B_z, which is shown in Fig. 2(a) as a dotted line. If any flux jumps can be avoided, the B_z value over 0.9 T can be realized as shown in Fig. 2(a). The typical trapped field profiles are shown in Figs. 2(a) and 2(b). For B_{ex} = 1.41 T, the profile is concave and nearly concentric because of the lower B_{ex}. On the other hand, for B_{ex} = 1.96 T, the profile is asymmetric and the magnetic flux can escape from the bulk center due to flux jumps.

The insets of Fig. 3 show the magnetization curves, which were calculated by $\Delta B = B_z(t) - B_{ex}(t)$. In the ascending stage of $B_{ex}(t)$, the magnetic flux can hardly penetrate into the bulk center and the ΔB value is nearly proportional to the negative applied field B_{ex} ($\Delta B = -B_{ex}$). A wide hysteresis loop can be seen clearly with increasing time, which mainly results from flux penetration and trapping in the bulk disk. A flux jump can be also confirmed in the hysteresis curve. Flux jump phenomena in the magnetic hysteresis measurement were frequently observed in the small MgB_2 samples at low temperature using a SQUID magnetometer [19, 20], where the temperature rise due to the flux jump quickly recovered and the magnetizing process started again over a long time scale. On the other hand, the escaped magnetic flux did not recover in the present PFM process using the large MgB_2 bulk: the magnetization process was finished within 0.1 s, but the elevated temperature did not recover to the initial temperature quickly.

Figure 4 presents the time dependence of the temperature, $T(t)$, during PFM on the side surface of the stainless steel ring for each applied field, B_{ex}. The maximum temperature, T_{max}, as a function of B_{ex}, is also shown in the inset. The temperature, $T(t)$, increases, takes a maximum at around t = 2 s, and then decreases with increasing time. Since the thermometer has a finite size, the measured temperature shows an average temperature change of the bulk disk within the ring.
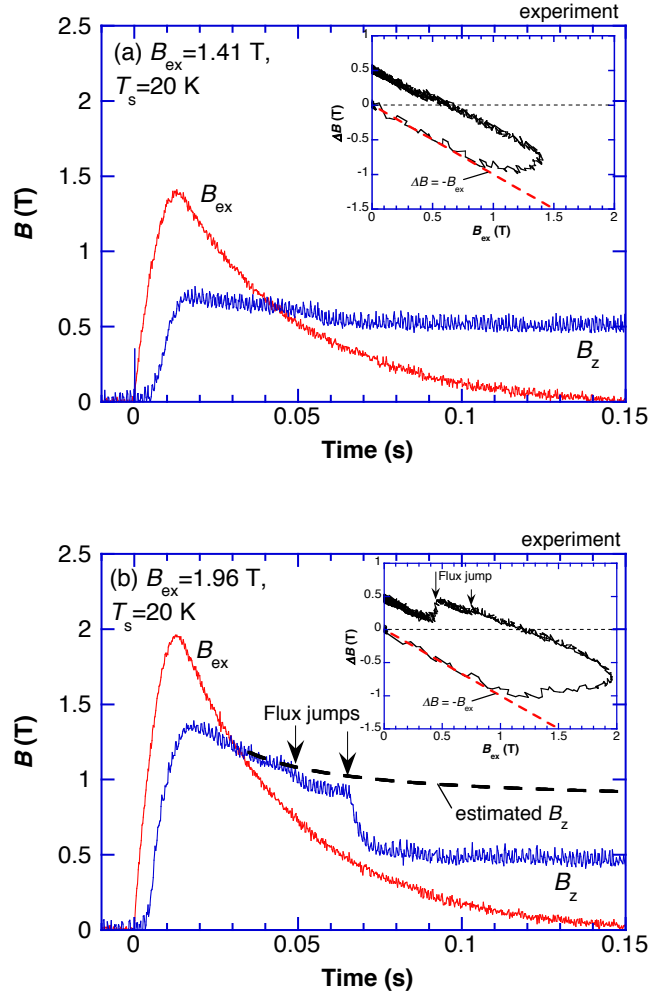
Figure 3. Time evolution of the local field, $B_z(t)$, at the center of the bulk surface and the applied pulsed field, $B_{ex}(t)$, for (a) B_{ex} = 1.41 T and (b) B_{ex} = 1.96 T at 20 K. The magnetization curves, which were calculated by $\Delta B = B_z(t) - B_{ex}(t)$, are shown in the insets.
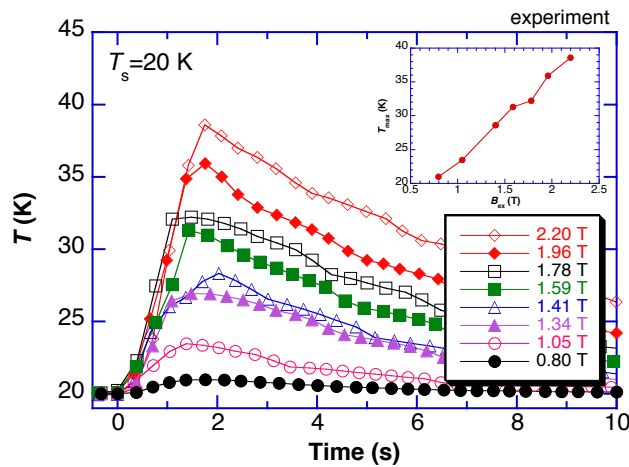

Figure 4. Time dependence of the temperature, $T(t)$, at the center of the bulk surface for each applied field, B_{ex}, during PFM. The maximum temperature, T_{max}, as a function of B_{ex}, is also shown in the inset.

Figure 5(a) shows the magnetic field dependence of the measured critical current density, $J_c(B)$, of the present MgB$_2$ bulk at T_s = 10, 20 and 30 K. J_c under zero field increases with decreasing temperature and J_c monotonically decreases with increasing magnetic field at each temperature. The values of J_c at 20 K are 4.3 x 10^9 A/m^2 at $\mu_0 H_a$ = 0 T and 3.1 x 10^8 A/m^2 at $\mu_0 H_a$ = 2 T, which are typically high J_c values in an MgB$_2$ bulks. Figure 5(b) shows the temperature dependence of the measured thermal conductivity, $\kappa(T)$, and the specific heat, $C(T)$, referred from [18] for bulk MgB$_2$. The $\kappa(T)$ value was as high as 18 W/mK at 20 K due to the higher mass density.
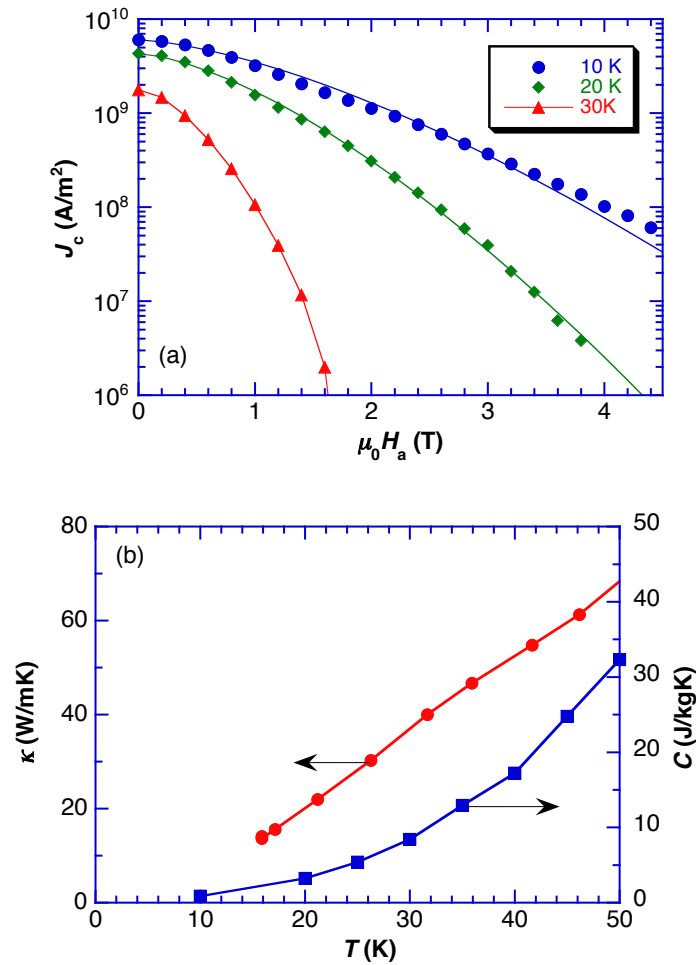

Figure 5. (a) Magnetic field dependence of the critical current density, $J_c(B)$, of the MgB$_2$ bulk under analysis at T_s = 10, 20 and 30 K. (b) Temperature dependence of the measured thermal conductivity, κ, and the specific heat, C, referred from [18] for bulk MgB$_2$.

4. Numerical Simulation Results

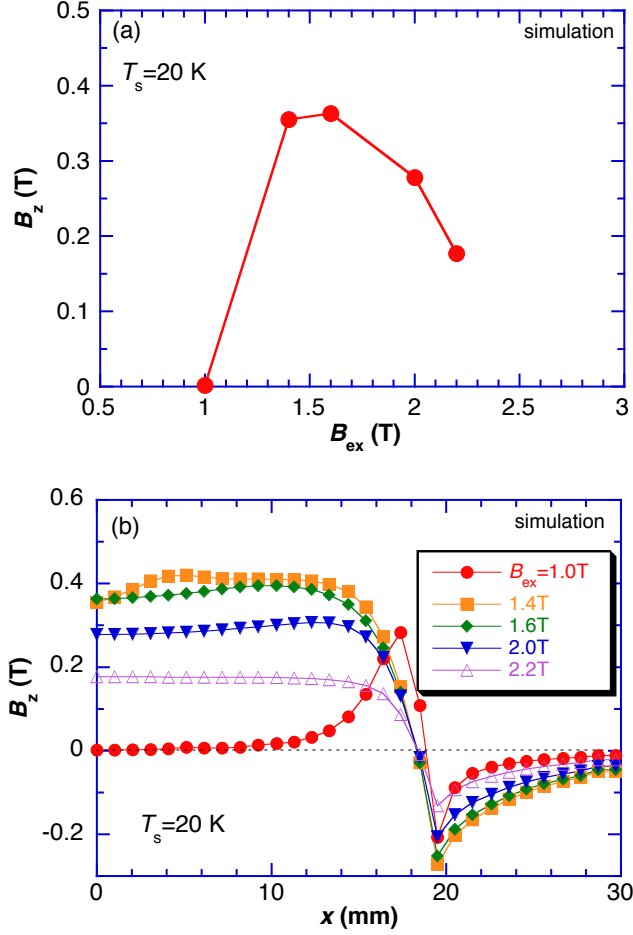Figure 6(a) depicts the results of the numerical simulation of the trapped field, B_z, at the center of the bulk surface, as a function of the applied field, B_{ex}, at 20 K. The B_{ex} vs. B_z profile using the numerical simulation qualitatively reproduces the experimental results shown in Fig. 2(a). However, the maximum B_z value is twice as large as that obtained in the

experiment, which may come from the overestimated κ_{cont} in the simulation compared to the actual κ_{cont} in the experiment. Figure 6(b) presents cross-sections of the trapped field profile, $B_z(x)$, for each B_{ex}. The $B_z(x)$ profile changes from concave for lower B_{ex} to trapezoidal for higher B_{ex}.

Figure 6. Numerical simulation results of the trapped field, B_z, at the center of the bulk surface, as a function of the applied field, B_{ex}, at 20 K. (b) Cross-sections of the trapped field profile, $B_z(x)$, for each B_{ex}.

5. Discussion

5.1 Estimation of critical thickness using experimental results

Here we discuss the magnetic instability during PFM using the conventional equations for superconducting wires [21]. In the classical slab model, the critical thickness, d_c, is usually used to evaluate magnetic instability. In order to avoid a flux jump or quench, a subdivision of the superconductor smaller than d_c is effective in minimizing flux movement. That is, d_c describes an upper safety limit of the thickness and can be written as follows,

$$d_c = 2\sqrt{\frac{3\gamma C(T_c - T)}{\mu_0 J_c{}^2}} \qquad\qquad (2)$$

where T_c is the transition temperature and T is the operating temperature. $J_c(T, B)$, $C(T)$ and γ are critical current density, specific heat and mass density (2360 kg/m^3) at T, respectively.

The minimum propagation zone (MPZ) length, l_m, is usually used to evaluate the dynamical instability under adiabatic conditions. If the superconductor is divided with the size below l_m, and is thermally connected to highly thermal conductive metal, the superconductor seems to be thermally stable. l_m can be expressed using the following equation,

$$l_m = \sqrt{\frac{2\kappa(T_c - T)}{\rho J_c{}^2}} \qquad\qquad (3)$$

where $\kappa(T)$ is the thermal conductivity and ρ is the normal state resistivity just above T_c.

Figure 7 shows the temperature dependence of the critical thickness, d_c, of the present MgB$_2$ bulk for each magnetic field, which is calculated using the $J_c(T, B)$ and $C(T)$ values shown in Fig. 5. These results suggest a maximum thickness of 0.86 mm, when the present MgB$_2$ bulk is carrying its critical current, above 20 K and above 1 T [22], which is about one order of magnitude shorter than that for the GdBaCuO bulk (d_c = 4.9 mm at 40 K and 1 T) [11]. This suggests that the MgB$_2$ bulk at 20 K is magnetically unstable, compared with the GdBaCuO bulk at 40 K.
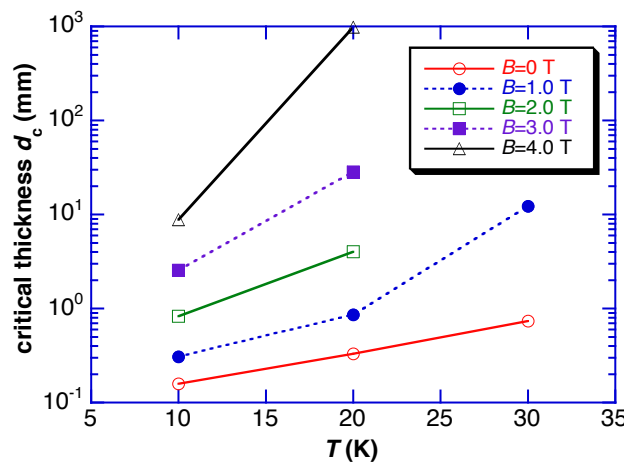

Figure 7. Temperature and magnetic field dependences of the critical thickness d_c for the present MgB$_2$ bulk.

5.2. Time dependence of critical thickness d_c and MPZ l_m using the results of numerical simulation

In subsection 5.1, the critical thickness d_c becomes longer with increasing temperature, T, and magnetic field, B, which implies flux jumps are less likely to happen during PFM. However, flux jumps often happen for higher applied fields, B_{ex}. Inhomogeneous heat generation takes place adiabatically over a short time period in the disk-shaped bulk. We suppose that the flux jump mainly results from a local temperature rise above T_c and calculate the time dependence of the critical thickness, $d_c(t)$, using the $T(t)$ estimated by the numerical simulation at three typical points (center: $(x, z) = (0, 0)$, middle: $(8, 0)$ and side: $(17, 0)$) in the bulk disk, as shown in Fig. 8.

Figure 9 presents the estimated time dependence of the temperature, $T(t)$, at these three positions after applying a pulsed field of $B_{ex} = 1.6$ T at 20 K, at which the trapped field takes a maximum, as shown in Fig. 6(a). The time dependence of $B_{ex}(t)$ is also shown on the right vertical axis. The temperature rise starts to increase from the bulk periphery due to the flux penetration. At the side of the bulk, $(x, y) = (17, 0)$, $T(t)$ exceeds $T_c = 39$ K at $t = 0.009$ s and decreases below T_c at $t = 0.04$ s. The time, at which $T(t)$ exceeds T_c and recovers to below T_c, is delayed for the middle and the center positions of the bulk in this order.

Figure 10 shows the time dependences of the temperature, $T(t)$, critical current density, $J_c(t)$, specific heat, $C(t)$, and critical thickness, $d_c(t)$, at the center position, $(x, y) = (0, 0)$, for $B_{ex} = 1.6$ T at 20 K. $d_c(t)$ was calculated using Eq. (2). $J_c(t)$ decreased and $C(t)$ increased with increasing time due to the temperature rise, both of which contribute the increase of d_c. In order to decrease the value of d_c and to induce a flux jump, $T(t)$ must be increased and exceed T_c. In this case, the flux jump should take place at the bulk center at $0.03 \leq t \leq 0.08$ s. Even if the temperature, $T(t)$, recovers below T_c at $t > 0.08$ s, the trapped field cannot be recover to the previous value because it takes much time to recover the initial temperature and the pulsed field, $B_{ex}(t)$, has decreased significantly by this time. In the PFM experiments shown in Fig. 3, the flux jumps almost always happen during the descending stage of the magnetic pulse (*i.e.*, $t > 0.02$ s).

Figure 11 shows the time dependence of the estimated $d_c(t)$ at the three positions for $B_{ex} = 1.6$ T at 20 K. The value of $d_c(t)$ for the center position is also reused. If the flux jump is supposed to take place during the time when $T(t) > T_c$, the position at which the flux jump happens proceeds from the side to the center of the bulk with increasing time. Figure 12 presents the time dependence of the MPZ length, $l_m(t)$, at the three positions for $B_{ex} = 1.6$ T at 20 K, which was calculated using Eq. (3). The value of $l_m(t)$ is about one order of magnitude smaller than $d_c(t)$, which suggests that the MgB$_2$ bulk is thermally unstable, rather than magnetically. These analyses suggest a possible approach to understand and avoid this flux jump behavior. The use of a longer applied pulsed field and a powerful and stable cooling apparatus for the bulk is a valuable approach to avoid flux jumps because it restricts the

$a = b$ temperature rise [16]. The use of a concentric-circled MgB$_2$ bulk composite disk, which consists of many MgB$_2$ thin rings in the highly thermally conductive metal disk, is also another potentially valuable solution to avoid flux jumps caused by PFM [15].
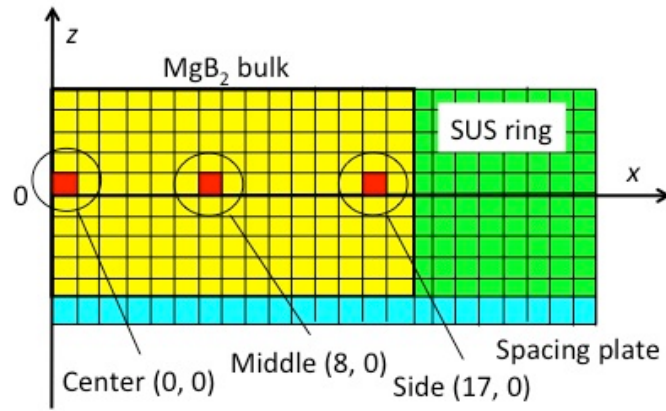

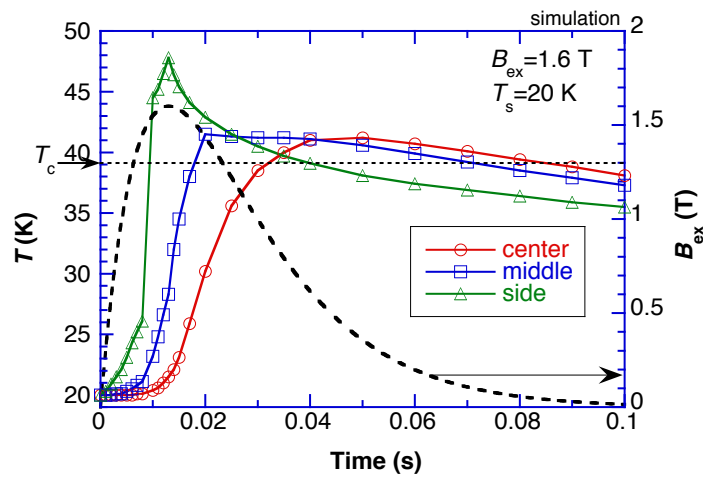Figure 8. The positions for the calculation of the time dependence of d_c and l_m.

Figure 9. Estimated time dependence of the temperature, $T(t)$, at the three positions (center, middle, side) after applying a pulsed field of B_{ex} = 1.6 T at 20 K, which were obtained by numerical simulation.
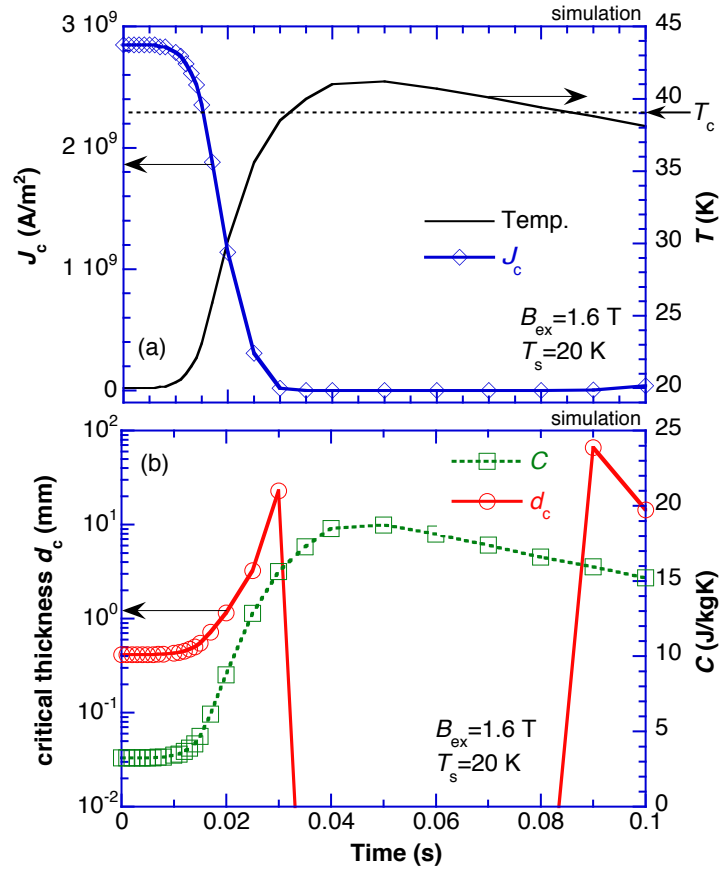
Figure 10. Estimated time dependence of the temperature, $T(t)$, critical current density, $J_c(t)$, specific heat, $C(t)$, and critical thickness, $d_c(t)$, at the center position for B_{ex} = 1.6 T at 20 K. $d_c(t)$ was calculated using Eq. (2).
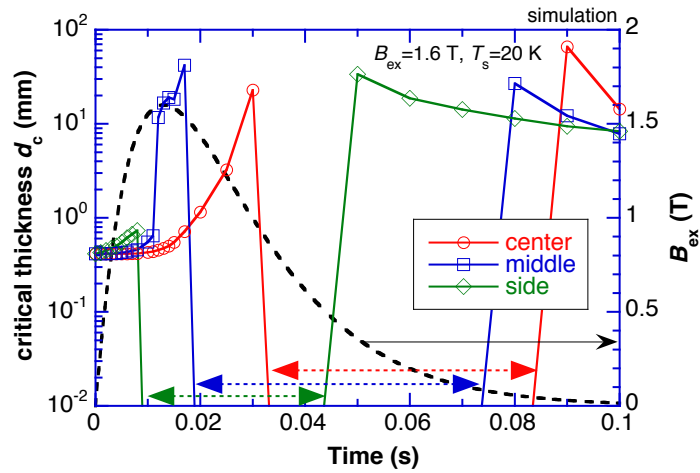

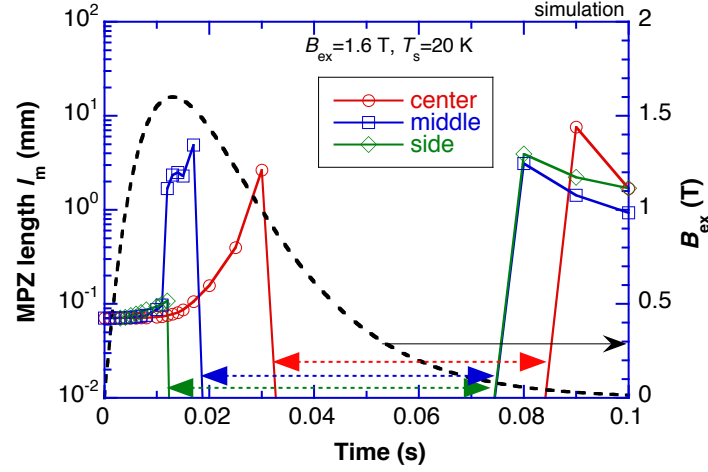Figure 11. Time dependence of the estimated $d_c(t)$ at the three positions for B_{ex} = 1.6 T at 20 K.

Figure 12. Time dependence of the estimated $l_m(t)$ at the three positions for B_{ex} = 1.6 T at 20 K. $l_m(t)$ was calculated using Eq. (3).

6. Conclusion

Pulsed field magnetization (PFM) of a high-J_c bulk MgB_2 disk has been investigated experimentally, in which flux jumps frequently occur for higher pulsed fields, B_{ex}. Using a numerical simulation of the PFM procedure, we estimated the time dependence of the local magnetic field and temperature during PFM, and analyzed the electromagnetic and thermal instability of the high-J_c MgB_2 bulk to avoid the flux jump using the time dependence of the critical thickness, $d_c(t)$, and the minimum propagation zone (MPZ) length, $l_m(t)$. The values of $d_c(t)$ and $l_m(t)$ change along the thermally stabilized direction with increasing temperature below the critical temperature, T_c. However, the flux jump behavior can be qualitatively understood by the local temperature, $T(t)$, which exceeds T_c in the bulk. The use of a longer applied pulsed field and a powerful and stable cooling apparatus for the bulk is are valuable approaches to avoid flux jumps because it restricts the temperature rise.

References

[1] Kambara M, Babu N H, Sadki E S, Cooper J R, Minami H, Cardwell D A, Campbell A M and Inoue I H 2001 *Supercond. Sci. Technol.* **14** L5

[2] Durrell J H, Dancer C E J, Dennis A, Shi Y, Xu Z, Campbell A M, Hari N, Todd R I, Grovenor C R M and Cardwell D A 2012 *Supercond. Sci. Technol.* **25** 112002

[3] Yamamoto A, Ishihara A, Tomita M and Kishio K 2014 *Appl. Phys. Lett.* **105** 032601

[4] Naito T, Yoshida T and Fujishiro H 2015 *Supercond. Sci. Technol.* **28** 095009

[5] Fuchs G, Häßler W, Nenkov K, Scheiter J, Perner O, Handstein A, Kanai T, Schultz L and Holzapfel B 2013 *Supercond. Sci. Technol.* **26** 122002

[6] Yanagi Y, Itoh Y, Yoshikawa M, Oka T, Hosokawa T, Ishihara H, Ikuta H and Mizutani U 2000 *Advances in Superconductivity* vol. 12 (Tokyo: Springer) p 470

[7] Sander M, Sutter U, Koch R and Klaser M 2000 *Supercond. Sci. Technol.* **13** 841

[8] Fujishiro H, Tateiwa T, Fujiwara A, Oka T, and Hayashi H 2006 *Physica C* **445–448** 334

[9] Fujishiro H, Tamura T, Arayashiki T, Oyama M, Sasaki T, Naito T, Giunchi G and Albisetti A F 2012 *Jpn. J. Appl. Phys.* **51** 103005

[10] Fujishiro H, Ujiie T, Naito T, Albisetti A F and Giunchi G 2014 *J. Phys. Conf. Series* **507** 032016

[11] Fujishiro H, Ujiie T, Mochizuki H Yoshida T and Naito T 2015 *IEEE Trans. Appl. Supercond.* **25** 6800104

[12] Ainslie M D, Fujishiro H, Ujiie T, Zou J, Dennis A R, Shi Y-H and Cardwell D A 2014 *Supercond. Sci. Technol.* **27** 065008

[13] Ainslie M D and Fujishiro H 2015 *Supercond. Sci. Technol.* **28** 053002

[14] Zou J, Ainslie M D, Fujishiro H, Bhagurkar A G, Naito T, Hari Babu N, Fagnard J-F, Vanderbemden P and Yamamoto A 2015 *Supercond. Sci. Technol.* **28** 075009

[15] Mochiduki H, Fujishiro H, Naito T, Albisetti A F and Giunchi G 2015 *Supercond. Sci. Technol.* **28** 105004

[16] Fujishiro H and Naito T 2010 *Supercond. Sci. Technol.* **23** 105021

[17] Fujishiro H, Naito T and Yoshida T 2014 *Supercond. Sci. Technol.* **27** 065019

[18] Wang Y, Plackowski J and Junod A 2001 *Physica C* **355** 179

[19] Romero-Salazar C, Morales F, Escudero R, Duran A, Hernandez-Flores O A 2007 *Phys. Rev. B* **76** 104521

[20] Kimishima Y, Takami S, Okuda T, Uehara M, Kuramoto T and Sigiyama Y 2007 *Physica C* **463-465** 281

[21] Wilson M *"Superconducting Magnets"*, 1983, p. 131. Oxford Sci. P. Ed.

[22] Giunchi G 2006 *Advances in Cryogenic Engineering: Transactions of the International Cryogenic Materials Conference – ICMC*, **52** 813